An Integrated Wind Resource Assessment Tool for Wind Farm Planning: System's Upgrades and Applications

Giovanni Gualtieri*‡

*National Research Council–Institute of Biometeorology (CNR–IBIMET),

Via Caproni 8, 50145 Firenze, Italy

‡Corresponding Author; Address:Via Caproni 8, 50145 Firenze, Italy, Tel: +39 55 3033743

Fax: +39 55 308910, g.gualtieri@ibimet.cnr.it

Received: 04.07.2016 Accepted:16.08.2016

Abstract- An integrated wind resource assessment tool (WRAT) was previously developed and tested to support wind energy studies during the pre-feasibility stage. This WRAT was applied across a 4-year period to assess the wind potential of the Tuscany region (Italy) according to a 2-km spatial resolution based on 120x107 (12840) gridded points. This application provided the input to a GIS-based interactive web decision support system aimed at wind farm planning in Tuscany.
In the present work all significant upgrades implemented to the WRAT are described, as well as their main on-site applications performed within wind energy studies in the recent literature. Main WRAT upgrades include: (i) integration of further wind turbine models into system's database; (ii) wind power density function; (iii) wind speed vertical extrapolation based on logarithmic law and power law; (iv) annual energy yield uncertainty assessment; (v) wind data import and processing at 10-min time bin; (vi) computation of wind turbulence parameters such as turbulence intensity and gust factor; (vii) turbulence intensity vs. wind speed plot and compliance assessment to the IEC standards. In the end, a number of system's limitations are also pointed out, as well as further upgrades to be possibly implemented in the near future to overcome some of those limitations.

Keywords- Wind resource assessment tool; Wind farm planning; Wind speed vertical extrapolation; Turbulence parameters; Energy yield uncertainties.

1. Introduction

Several software packages are commercially available to help wind analyzers perform an accurate wind resource assessment of a site and achieve the most efficient and economical wind farm layout. Among others, a list of the currently most popular ones includes: WindSim [1], WAsP [2],WindFarmer [3], WindPRO [4], and WindFarm [5]. In general, these packages integrate specific modules designed to perform data mining, 3D wind field reconstruction and wind turbine (WT) wakes assessment – often based on computational fluid dynamics (CFD) models –, wind resource and energy yield assessment, wind farm layout optimization, project's financial analysis, electric grid connection, environmental (visual, noise, shadow flicker, bird collisions) impacts, etc. They are generally provided by an exhaustive and updated WT archive, and are often conceived to ingest the output from numerical weather prediction (NWP) models such as, e.g., the Weather Research Forecast (WRF) model [6]. Therefore, as well as quite easy to be used, these softwares are capable of performing accurate wind resource assessments – thus minimizing project's financial risks –, returning quick responses – thus minimizing time consumption –, and in general comprehensively addressing all main aspects involved in all various stages of a wind farm project. However, from a strictly research viewpoint, they come up with some shortcomings, including: (i) the relevant licence cost for purchase, technical support and upgrade, also to be renewed across the years; (ii) the fact they are not open to be customized so as to implement routines/algorithms addressing specific research issues. Actually, the cost for

academic/educational licences is typically a significantly reduced amount of the full cost required for commercial purposes. In the same time, various tools are also available on the net to be downloaded and used for free, e.g.: WRPLOT [7], to calculate windrose plots and wind speed frequency distributions; Hybrid Optimization Model for Electric Renewable (HOMER) [8], to optimize design of a renewable energy system for both grid-connected and off-grid power systems; RETScreen [9], to address a complete wind energy project's financial analysis. Recent applications of these tools may be found in the works by Rahmani et al. [10] (WRPLOT), Goel and Ali [11] (HOMER), Soe et al. [12] and Acakpovi [13] (RETScreen). Very useful wind energy calculators are also available online, such as, among others, the one developed at the Danish Wind Industry Association website [14], or the one available at the Swiss wind power data website [15]. In any case, as apparent, these freeware tools are only capable of addressing specific aspects of a wind farm project – not all of them.

Due to all these reasons, in the research community it is often preferable to internally develop custom tools/facilities, which have therefore the advantage of being open-source, modular, inexpensive and easy to be used. Computer programs conceived as integrated tools to thoroughly calculate and analyse wind resource potential and expected energy production of a site have been purposely developed across the years. For example, based on local weather data and typical WT characteristics, Lu et al. [16] proposed a simulation model for calculating wind speed probability density and wind power density for Hong Kong islands. Al-Mohamad and Karmeh [17] developed a computer program, written in C++ language, for calculating wind energy potential and possible generated electricity in Syria using the available meteorological data (more than 20 stations) provided by the Syrian Atlas. Bhuiyan et al. [18] developed a web software which was used to assess the wind potential and energy generation in Bangladesh based on a sample 1-kW WT.

An integrated wind resource assessment tool (WRAT) was developed earlier aimed at supporting wind energy studies during the pre-feasibility stage [19]. This WRAT was applied to calculate the wind potential of the Tuscany region (Italy), based on 1-h wind field estimations provided by the coupled WRF and CALMET [20] models at 2-km resolution using a computation grid made of 120x107 (12840) points. The WRAT was applied over a 4-year time period (2004–2007, 35064 hours). This application also provided the input to a GIS-based interactive web decision support system purposely developed as a guide for wind farm planning in Tuscany [21]. The goal of present work is to describe all significant upgrades implemented to the WRAT with respect to its previous version, as well as to report their main on-site applications carried out within wind energy studies in the recent literature.

2. Methods

2.1. Wind power density function

For an area A [m^2] of the WT rotor disc and a given wind speed v [m/s], site's available wind power $P(v)$ [W] is [22]:

$$P(v) = \frac{1}{2} \rho A v^3 \quad (1)$$

where ρ [kg/m^3] is the air density. $P(v)$ is the kinetic energy per unit time of wind flow potentially available at the site [23]. Wind power per unit area, or wind power density (PD) [W/m^2], is the kinetic PD (PD_k, total power input):

$$PD = PD_k = \frac{P(v)}{A} = \frac{1}{2} \rho v^3 \quad (2)$$

According to the Betz' law, maximum power that can be theoretically extracted from the wind, $P_{Betz}(v)$, is 16/27=59% of $P(v)$ [22]. Therefore, the Betz PD (PD_{Betz}) is:

$$PD_{Betz} = PD_m = \frac{P_{Betz}(v)}{A} = \left(\frac{16}{27}\right) \frac{1}{2} \rho v^3 \quad (3)$$

PD_{Betz} is also a site-specific quantity, representing the PD_k fraction that can be theoretically converted by an ideal WT to mechanical PD (PD_m, usable power input).

Multiplying, for each v bin, site's v probability density function $f(v)$ by the WT electric power curve $P_e(v)$ divided by its area A, it is possible to calculate the PD_m fraction that can be actually converted by the WT into electric PD (PD_e, total power output):

$$PD_e = \frac{P_e(v)}{A} f(v) * F_L \quad (4)$$

where F_L [%] is a factor accounting for total power losses.

2.2. Wind energy output

Based on $P_e(v)$ and assuming $\bar{t}$ =8760 hours, the net Annual Energy Yield (*AEY*) [kWh/y] produced by a WT over a 1-year period is [18]:

$$AEY = \bar{t} \int_{v_i}^{v_o} P_e(v) f(v) dv * F_L \quad (5)$$

where v ranges between WT's cut-in (v_i) and cut-off (v_o) wind speeds.

Capacity factor (*CF*) [%] is the ratio of *AEY* to the energy (E_r) [kWh/y] that the WT could have been produced if operated at its rated power over the same period [18]:

$$CF = \frac{AEY}{E_r} \quad (6)$$

Full-Load Hours (*FLH*) [h/y] are obtained by multiplying *CF* by the number of hours in one year ($\bar{t}$ =8760) [19]:

$$FLH = CF * \bar{t} = CF * 8760 \quad (7)$$

2.3. Wind speed vertical extrapolation

Two mathematical models are commonly used to quantify wind speed vertical profile over regions of homogeneous, flat terrain: the logarithmic law (LogL) and the power law (PL) [24].

According to the LogL, wind speed v at height z [m] is given by [24]:

$$v(z) = \frac{u_*}{\kappa} ln\left(\frac{z}{z_0}\right) \quad (8)$$

where κ is the von Karman's constant (typically 0.4), u_* the friction velocity [m/s], and z_0 the roughness length [m]. The LogL is a physical model that can be theoretically derived from basic principles of fluid mechanics [24]. It is actually only valid under near-neutral (adiabatic) stability conditions, near the ground over a relatively smooth surface [25].

From v_1 measurements at height z_1, v_2 at height z_2 can be estimated by transforming Eq. (8):

$$v_2 = v_1 \frac{ln(z_2 / z_0)}{ln(z_1 / z_0)} \quad (9)$$

The PL is a simple model expressed by [24]:

$$v_2 = v_1 \left(\frac{z_2}{z_1}\right)^{\alpha} \quad (10)$$

where v_1 and v_2 are wind speeds at heights z_1 and z_2, respectively. The adimensional exponent α is a highly varying parameter [23], as strongly depending both on site and on time [26]. It depends on v [27], z_0 [28], atmospheric stability conditions [29], and the height range [30]. In practice, the exponent α is the PL equivalent of z_0 to LogL [27]. Eq. (10) is an engineering approximation based on finding the magnitude of the exponent α [31], and thus, by contrast to the LogL, an empirical model [32]. It is generally valid up to 200 m from the ground [24].

In Table 1 the typical values of z_0 and α as a function of landscape type, and thus of roughness class, are reported to be used for applying the LogL (Eq. 9) and PL (Eq. 10), respectively.

Table 1. Roughness classes and z_0 considered by the Danish Wind Industry Association [14], and corresponding α values based on literature surveys (e.g. [28])

Roughness class	Landscape type	z_0 (m)	α
0	Water surface	0.0002	0.10
0.5	Completely open ground with a smooth hard ground	0.0024	0.10
1	Open farming areas with scattered buildings; rounded hills	0.03	0.15
1.5	Farming land with a frew houses; grassland	0.055	0.15
2	Farming land with some houses; tall crops, hedges and shrubs	0.1	0.22
2.5	Farming land with many houses, shrubs and plants	0.2	0.22
3	Small towns; farming land with many tall hedges; forested areas	0.4	0.30
3.5	Large cities with high rise buildings; hevily forested areas	0.8	0.30
4	Very large cities with high rise buildings	1.6	0.40

2.4. Turbulence intensity

Wind turbulence refers to fluctuations in wind speed on a relatively fast time-scale, typically less than about 10 min [33]. Wind turbulence generation is basically driven by both mechanical and thermal effects: mechanical turbulence depends on friction with ground surface and on topographical structures such as hills and mountains, while thermal turbulence is due to convective temperature (and thus air density) variations which can cause air masses to move vertically [33].

A thorough knowledge of wind turbulence is important because it causes random, fluctuating loads and power output, and stresses over the whole WT and tower structure [23]. As a matter of fact, turbulence leads to an increase in: (i) energy losses, thus directly impacting on *AEY* [33]; (ii) *AEY* uncertainties, basically due to WT power curve uncertainty [34]; (iii) fatigue loads on WTs, thus reducing WTs operational life [35].

Turbulence intensity (I) [%] is a commonly accepted indicator in wind energy studies to measure the overall level of turbulence of a site. It is defined as [33]:

$$I = \frac{\sigma_u}{\bar{v}} \quad (11)$$

where σ_u is the standard deviation of longitudinal v fluctuation, and $\bar{v}$ is the average mean v. Both σ_u and $\bar{v}$ are calculated over 10-min bins.

I as defined in Eq. (11) is also known as ambient turbulence intensity (I_0), thus highlighting that it only depends on site conditions. Indeed, when assessing the overall turbulence actually developed within a wind farm, an additional turbulence intensity (I_+) should be considered due to wake interferences occurring between neighbouring WTs. These wake effects result in both wind speed decrease (deficit) and turbulence increase. Resulting energy reduction in a wind farm because of wake can be in the range 2–20% depending on distances between WTs and on ambient turbulence [36]. Summarizing, total turbulence intensity (I_T) within a wind farm can be calculated from [36]:

$$I_T^2 = I_0^2 + I_+^2 \quad (12)$$

2.5. Gust factor

A wind gust is defined by its magnitude, duration and frequency of occurrence [24]. When extreme wind speeds occur at a site, for safety purposes WTs are automatically shut down and disconnected from the grid, which may results in relevant power output reduction. To this aim, it is useful to know the maximum gust speed that can be expected to occur in any given time interval. This is usually represented by mean gust factor *G*, an adimensional parameter defined as [33]:

$$G = \frac{v_g}{\bar{v}} \quad (13)$$

where v_g is the average wind speed during the gust over a 10-min bin.

G is a direct function of *I* and an inverse function of gust duration [24]. Clearly, extreme wind gusts (both in terms of magnitude and shape) may be quite site-specific: for example, they may differ considerably between flat coastal sites and rugged hill-tops [33]. Indeed, experimental studies (e.g. [37–38]) demonstrated that stronger gusts are associated with lower mean speeds.

2.6. Energy yield uncertainties

To preliminary assess financial viability of a wind energy project, a careful analysis of all uncertainties associated with expected wind farm energy production is mandatory [36]. Actually, estimation of wind resource is a greatly uncertain process, typically affected by unavoidable errors which eventually sum up into *AEY* computation [39]. The error in estimating *AEY* is assumed exhibiting a Gaussian probability density function, where *AEY* (=AEY_{50}, Eq. 5) is the mean value (μ) and U_{AEY} (total uncertainty) is the standard deviation (σ). Therefore, starting from AEY_{50} (*AEY* with a 50% probability of occurrence in a year), it is possible to reconstruct the full probability distribution, with particular attention to AEY_{75} and AEY_{90} (*AEY* with 75 and 90% probability of occurrence in a year, respectively), which are the other two producibility parameters typically taken into account during the wind energy project feasibility stage. Thus, AEY_{75} could be considered as the (intermediate) "base-case" between the AEY_{50} (too optimistic) "best-case" and the AEY_{90} (too pessimistic) "worst-case". As well as referred to *AEY*, the same uncertainty Gaussian probability distribution can be referred to Full-Load Hours (*FLH*, Eq. 7), i.e. FLH_{50}, FLH_{75} and FLH_{90}.

Total uncertainty in estimating *AEY* (U_{AEY}) is [39]:

$$U_{AEY} = \sqrt{\sum_i U_i^2} \quad (14)$$

where U_i are values related to single uncertainty components.

Typically, uncertainty values may be associated to either *v* estimation, or *AEY* estimation itself: *v*-related uncertainties include those associated to *v* measurements (when using sensors) or estimates (when using NWP models), data recovery, data duration and availability, Weibull probability density function, vertical extrapolation, etc.; *AEY*-related uncertainties include those associated to site's topography complexity, WT power curve, WT wakes modelling, etc. Table 2 gives a summary of main *AEY* uncertainty components and their typical ranges based on the literature [36,40–42].

Theoretically, AEY_{50} can be used when U_{AEY} is below 10%, AEY_{75} when U_{AEY} is between 10 and 20 %, and AEY_{90} when U_{AEY} is above 20%. However, from a financial point of view, in practice AEY_{75} and AEY_{90} are preferably used in order to minimize the project's risks, thus applying an acceptable safety margin [43].

Table 2. *AEY* uncertainty components and their typical range based on works in the literature [36,40–42]

Uncertainty component	U_i typical range	
	% of wind speed	% of *AEY*
Wind speed measurement or estimation	6.0–12.0	
Measurements/estimations time span (long-term correction)	3.0–5.0	
Measurements/estimations availability	2.0–4.0	
Wind speed Weibull distribution	2.0–5.0	
Wind speed vertical extrapolation	2.0–4.0	
Air density assessment		2.0–4.0
Site's topography complexity (wind spatial extrapolation)		2.0–8.0
WT power curve		4.0–6.0
Wake interferences between WTs		1.0–2.0
Other		1.0–2.0

3. Description of System's Upgrades

With respect to the previous WRAT version described in [19], the following upgrades have been implemented: (i) integration of further WT models into the system's database; (ii) wind power density function; (iii) *v* vertical extrapolation based on LogL and PL; (iv) *AEY* uncertainty assessment; (v) wind data import and processing at 10-min resolution; (vi) computation of wind turbulence parameters such as *I* and *G*; (vii) *I* vs. *v* plot and compliance assessment with the IEC standards [44]. As concerns (i), total number of integrated WTs has been increased from 200 to 350. The substantial change of system's structure following the upgrade (v) enabled to implement all upgrades related to the wind turbulence assessment, i.e. (vi) and (vii).

Of course, all newly calculated parameters have been included in the MS Excel (.xls) output spreadsheet file generated by the WRAT, as well as in the output energy report dynamically drawn up – either in MS Word (.doc) document or (.html) web page format [19]. In the case of output energy report file, all newly implemented tables and plots have been also included. Furthermore, since the WRAT may be run in an automated (batch) mode for a large number of points over the study area [19], note that the newly implemented computations may also be performed in such a way, so as to be included in a dynamically generated all-inclusive spreadsheet file, where each record refers to any processed point.

4. System's Sample and Application Results

4.1. Wind power density function

Combining site's *v* data and power curve of the selected WT, the system calculates the PD function, as shown in Fig. 1. For each *v* bin, the following PD values [W/m^2] are provided: (i) site's kinetic PD potentially available at the site (PD_k, total power input, Eq. 2); (ii) the PD_k fraction that can be theoretically converted to mechanical PD based on the Betz' law (PD_m, usable power input, Eq. 3); (iii) the PD_m fraction that is actually converted by the WT to electric PD (PD_e, total power output, Eq. 4). For representation convenience, the *v* Weibull probability density function [%] is also plotted.

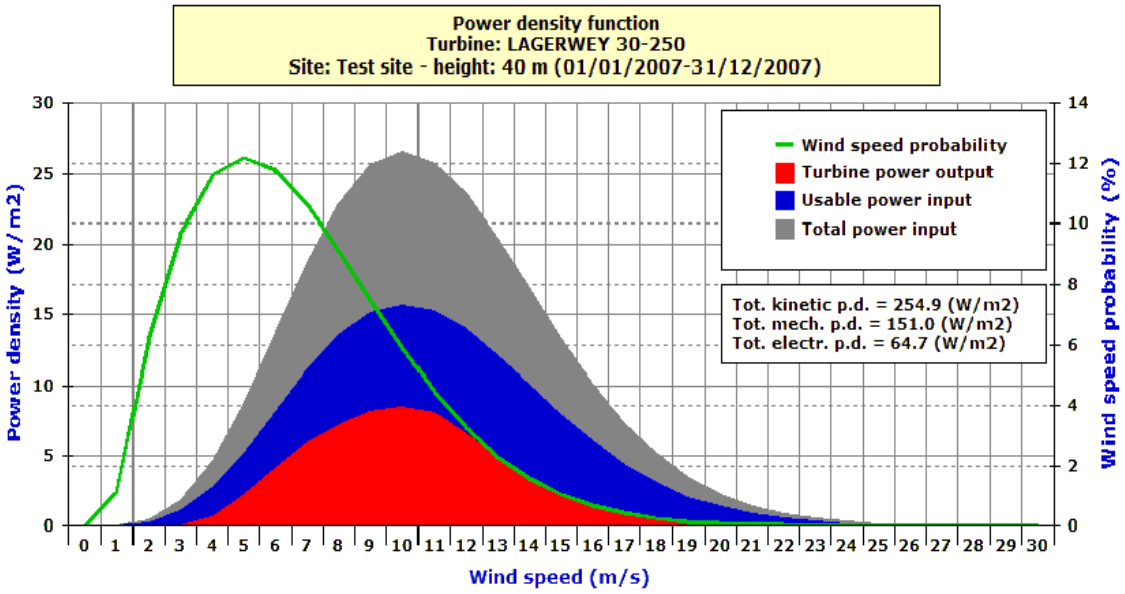

Fig. 1. System's sample: site's power density function, with associated Weibull wind speed probability density function.

From the graph it is straightforward to assess the usable power unit available for the site with respect to the total power unit (blue vs. grey areas), and then the fraction of usable power unit that is actually converted into electric power output by the WT (red vs. blue areas). By integrating each PD curve across its whole range, total corresponding amount is also returned. Summarizing, by means of a single, compact graph, both site wind resource potential and WT suitability to harness it can be obtained.

4.2. Wind speed vertical extrapolation

Based on available *v* measurements at lower height (e.g. 10 m), the system allows to easily extrapolate this resource to an upper level (typically, WT hub height) by using either the LogL (Eq. 9) or the PL (Eq. 10).

If the LogL option is chosen, the z_0 value is needed, while the α value is needed in the case of PL. These z_0 or α values are returned after the user selects the roughness class of the site, based on the lookup Table 1. The user may also

enter a user-defined value for either z_0 or α. As well as setting an overall (average) value of surface parameters quite representative for the site, a finer v extrapolation may be achieved by choosing a roughness class for each wind sector. As demonstrated in several works (e.g. [45]), this sector-wise v extrapolation returns finer scores than the one where a unique surface parameter is taken for the site.

In Fig. 2 a sample system's dialog of v extrapolation from 10 m to 45 m is shown, where in particular the PL applied with the varying wind direction option (by 16 sectors) has been selected.

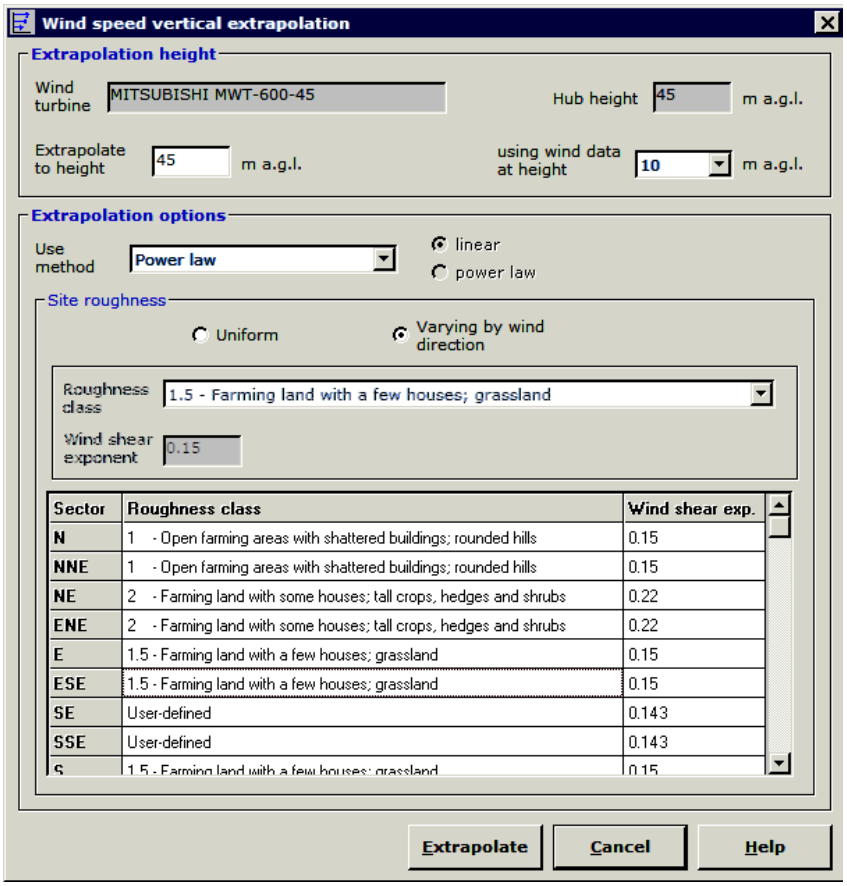

Fig. 2. Sample screen snapshot of system's wind speed vertical extrapolation dialog.

4.3. Turbulence intensity

Once wind data averaged to 10-min resolution are available, computation of turbulence parameters such as I (Eq. 11) and G (Eq. 13) is enabled. This system's facility has been employed, for example, in assessing the turbulence characteristics of four mountain sites along the Apennines chain in the Molise region, southern Italy, across a 2-year (2001–2002) period [46]. In Table 3 mean I values over these four sites at 30 m a.g.l. are presented, showing Serrazasilla being the site affected by the highest value (18.43%).

Table 3. System's application: statistical indicators of turbulence intensity and gust factor at 30 m observed at four sites in the Molise region, southern Italy (2001–2002) [46]

Parameter	Site			
	Serra della Spina	Toppo Cardeto	Costa Giardino	Serrazasilla
Mean I (%)	14.15	15.45	16.12	18.43
Mean G	1.33	1.36	1.37	1.42
Events with v_g > 25 m/s (%)	0.60	0.29	0.35	0.40
Maximum v_g (m/s)	44.30	36.35	41.10	42.55

Site's I values may also be represented through their frequency distribution. As shown in Fig. 3, based on 10-min measured data, the system was employed in assessing the I characteristics between 10 and 80 m at the site of Cabauw, the Netherlands, across a 1-year (2012) period [47]. In the histogram of Fig. 3, the most of I occurrences fall, on average, in the 10-15% bin. In the figure overall I mean values and standard deviations are also reported, showing that wind dataset at the lowest elevation (10 m) is affected – as expected – by the highest turbulence amount, while the opposite applies to the highest elevation (80 m).

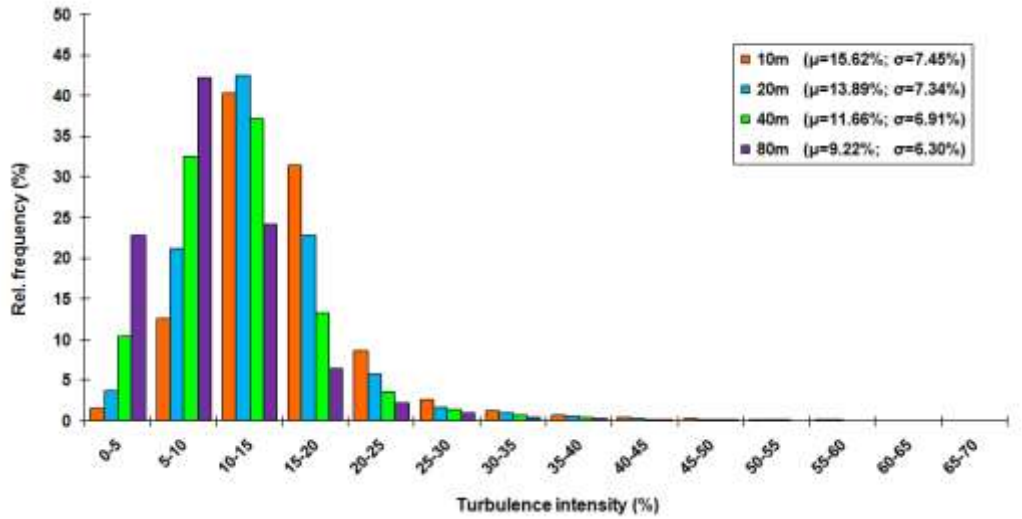

Fig. 3. System's application: histogram of 10-min turbulence intensity observed between 10 and 80 m at Cabauw, the Netherlands (2012), with overall mean values (μ) and standard deviations (σ) also reported [47].

Within the same Cabauw application, a further system's facility was used in deriving the scatter-plot by stability conditions of I vs. v observed at 40 m, as shown in Fig. 4. As expected, I decreases with v, though exhibiting a quite scattered pattern, particularly for stable and unstable conditions. Fig. 4 also shows the curves (I_u) for WT design for sites affected by higher (class A), medium (class B) or lower (class C) turbulence characteristics, as stated by the IEC 61400-1 standards [44]. Overall, the I curve of upper class A is exceeded by 0.3%. In terms of compliance with the IEC 61400-1 standards, mean I value at v=15m/s (11.26%) is lower than the expected turbulence intensity (I_{ref}) for WTs of class C (12%); thus, a class C, 40-m hub height WT could be suitable for the Cabauw site.

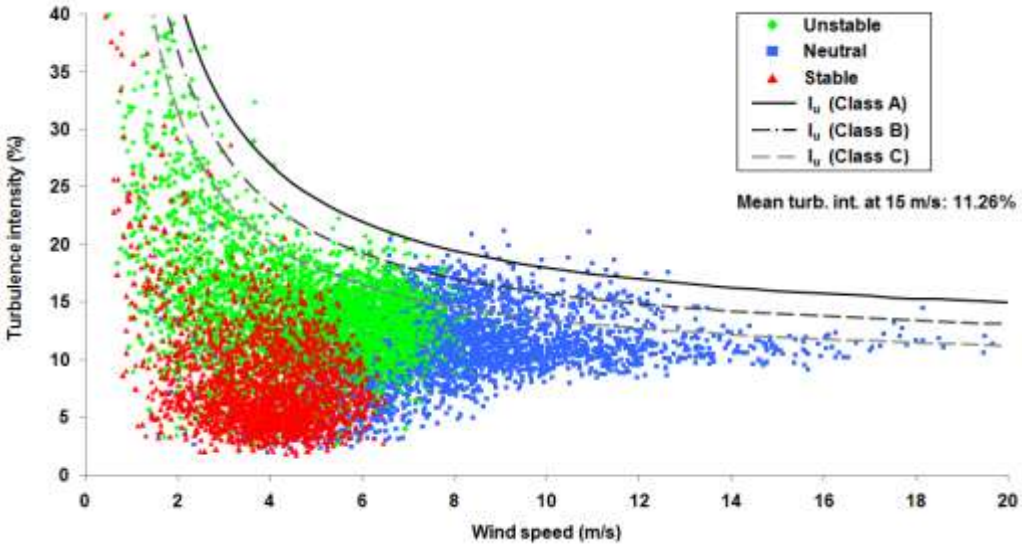

Fig. 4. System's application: scatter-plot by stability conditions of 1-h averaged turbulence intensity vs. wind speed observed at 40 m at Cabauw, the Netherlands (2012); the curves for WT design of turbulence classes A, B and C as stated by the IEC 61400-1 standards [44], as well as mean turbulence intensity at 15 m/s, are also shown [47].

A further useful system's facility in assessing site's turbulence aspects is the *I* rose, which shows mean *I* variation by wind sector. This option was used within the aforementioned application in the Molise region [46]. In particular, Fig. 5 shows the 10-min *I* values averaged to each of 16 wind sectors at the site of Serrazasilla at 30 m. Once overlapped over a site's detailed topography and/or landuse map, this *I* rose allows to easily and quickly detect those local surface features likely increasing or decreasing turbulence characteristics of the site.

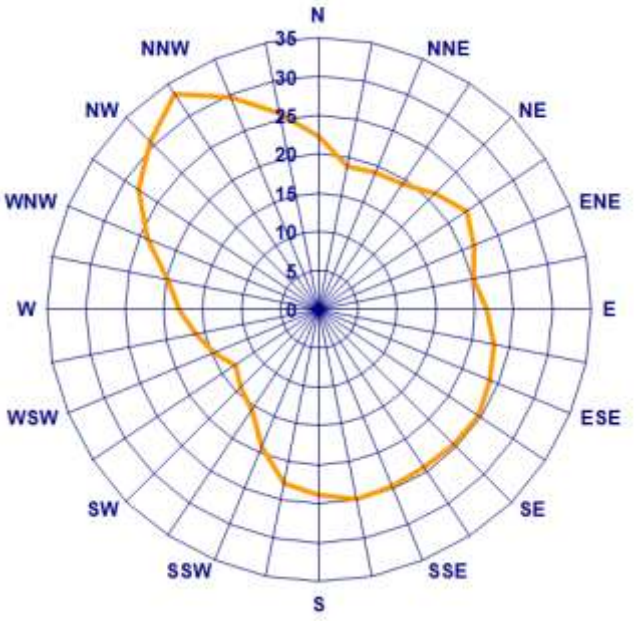

Fig. 5. System's application: variation by wind sector of 10-min turbulence intensity (%) observed at 30 m at the site of Serrazasilla, southern Italy (2001–2002) [46].

4.4. Gust factor

As mentioned above, at the four Molise sites *G* and v_g statistics at 30-m height were calculated, as summarized in Table 3. As expected not only based on theoretical results, but also on empirical ones [37], for each site mean *G* values are proportional to the corresponding mean *I* values: thus, the site of Serra della Spina is affected by the lowest mean *G* (1.33), while the site of Serrazasilla by the highest (1.42).

Maximum v_g values range between 36.35 and 44.30 m/s. The probability that v_g is higher than 25 m/s is quite negligible: 0.29–0.60%. Since v=25 m/s is the typical WTs' cut-off wind speed, this achieved percentage is useful to quantify the expected energy losses due to the WT disconnection from the grid for safety purposes.

The *G* frequency distribution is a further useful facility, as returned as an example in Fig. 6 for the site of Serra della Spina [46]. Herein, events with *G* values above 3.0 occurred by 0.17%.

Similarly to the *I* rose plot (Fig. 5), mean *G* variation by wind sector may also be calculated, as provided in Fig. 7, where the *G* rose for the same site of Serrazasilla was represented [46]. Although *I* and *G* mean values are proportional, it is apparent that the *G* sector variation (Fig. 7) is smoother than the corresponding *I* variation (Fig. 5).

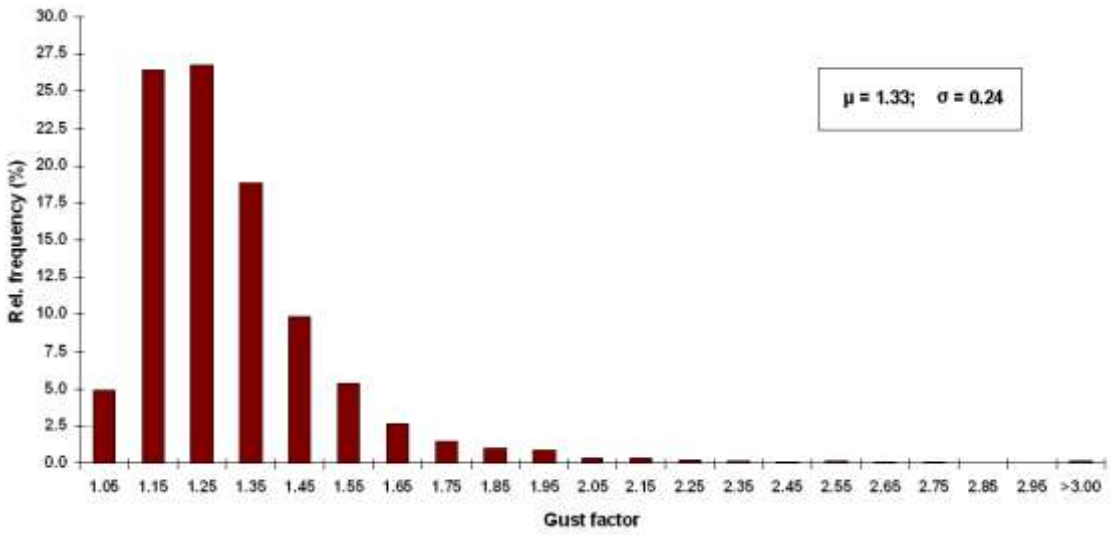

Fig. 6. System's application: histogram of 10-min gust factor observed at 30 m at the site of Serra della Spina, southern Italy (2001–2002), with overall mean (μ) and standard deviation (σ) also reported [46].

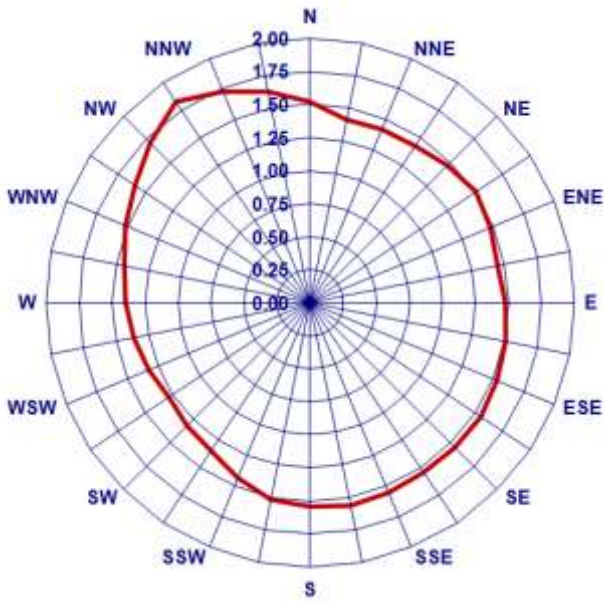

Fig. 7. System's application: variation by wind sector of 10-min gust factor observed at 30 m at the site of Serrazasilla, southern Italy (2001–2002) [46].

4.5. Energy yield uncertainties

A substantial system's upgrade was implemented in enabling a more thorough computation of actual net *AEY* by properly taking into account all possible uncertainty sources involved in the process. To this aim, for each uncertainty component the user is prompted by means of typical ranges suggested/recommended by the literature (such as those reported in Table 2), as well as being allowed to enter user-defined values based on his own experience.

Fig. 8 shows the system's settings dialog, markedly concerning tab of energy losses and energy uncertainties. Total energy uncertainties U_{AEY} are obtained as a quadratic sum of each component U_i based on Eq. (14), resulting equal to 12.41% in the case of Fig. 8.

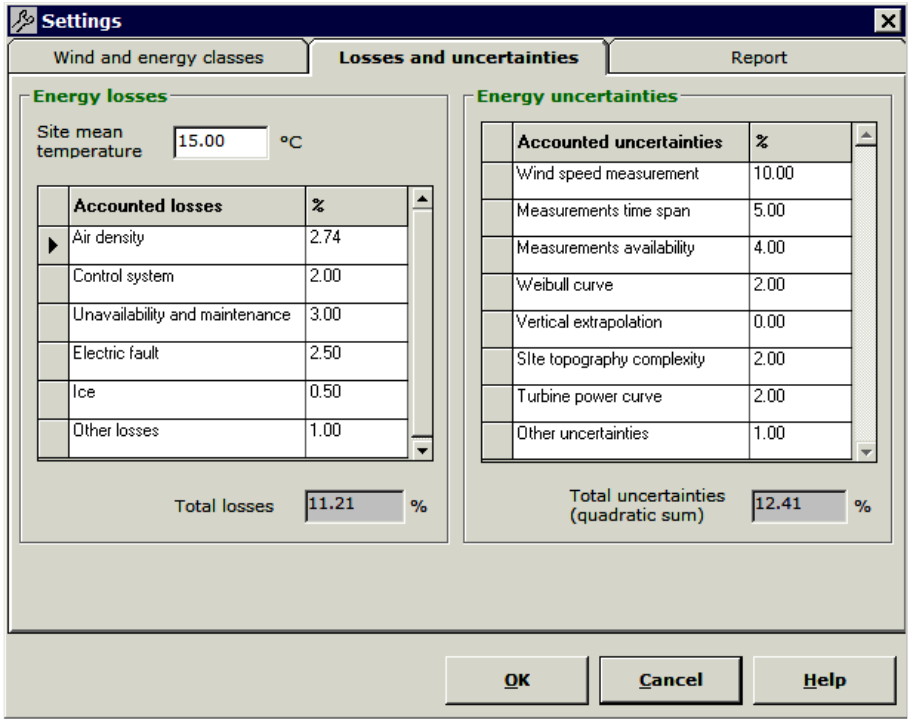

Fig. 8. Sample screen snapshot of system's settings dialog to manage energy losses and energy uncertainties.

After total energy uncertainties have been calculated (σ of the distribution), starting from the *AEY* value (μ of the distribution) the Gaussian probability density function associated to energy producibility is calculated. Because of the direct correspondence between *AEY* (Eq. 5) and *FLH* (Eq. 7), this probability density function may be represented in terms of either *AEY* or *FLH*.

Fig. 9 provides an example of *FLH* probability density function, associated to FLH_{50}=1603 h/y and 12.21% total uncertainties. Of course, the narrower the distribution around its mean value, the lower the energy uncertainty, and vice versa. In the case of Fig. 9, a conservative value of *FLH*=1460 h/y should be taken, corresponding to a 75% probability of occurrence.

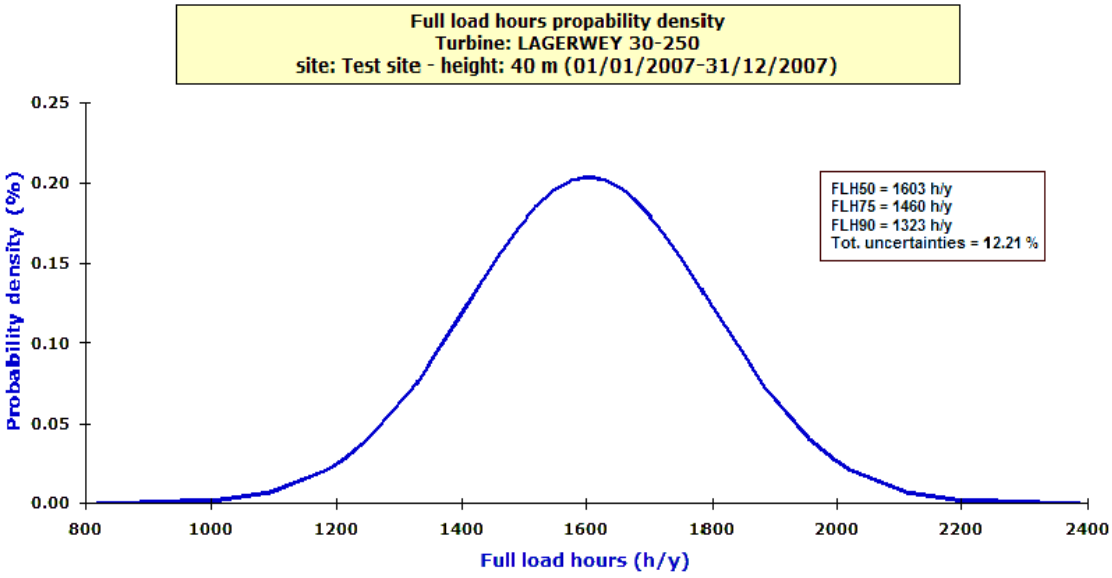

Fig. 9. System's sample: probability density function of full-load hours, with values of FLH_{50}, FLH_{75}, FLH_{90}, and total uncertainties also reported.

5. Conclusions and Perspectives

After a previous version was developed and tested, the WRAT was substantially improved after implementing a number of upgrades. Examples of on-site applications of the newly implemented upgrades carried out within various wind energy studies in the recent literature have been also presented.

Actually, various limitations still apply to the WRAT, due to the lack of specific modules to address the following issues:

(1) site's GIS-based survey geolocation, useful to both locate areas to be excluded (e.g. restricted areas, parks or natural sites, watercourses, urban sites, landscape constraints, too steep topography, etc.), and conversely areas to be attractively considered (e.g. areas quite close to electric grids);

(2) site's geophysical preliminary assessment, based on embedded high-resolution digital elevation model and landuse data, capable of returning surface parameters and surrounding topography structures of the site;

(3) high-resolution 3-D wind field reconstruction based on integrated CFD model;

(4) overall wind farm turbulence assessment based on integrated analytical wake model;

(5) wind farm layout optimization, primarily based on results from the wake model;

(6) wind project financial analysis;

(7) evaluation of fatigue loads on WTs and possible damage prediction;

(8) electric grid connection;

(9) environmental (visual, noise, shadow flicker, bird collisions) impacts.

In order to overcome some of limitations listed above, further system's upgrades should be implemented in the near future. For example, an analytical wake model to calculate the overall turbulence within the wind farm (point 4), and a wind farm layout optimization facility (point 5) strictly linked to the former appear among system's most urgent enhancements to be accomplished, as well as a tool to perform the wind farm economical analysis (point 6). Implementation of site's GIS-based geolocation facility (point 1) and integration with high-resolution digital elevation model and landuse data (point 2) are also foreseen, at least with limitation to specific regions of interest. Since the number of offshore WTs in the system's database is quite small (14 models), a further upgrade might concern addition of new offshore WTs into the database.

References

[1] WindSim, WindSim products, http://www.windsim.com/products/windsim-80.aspx, 2016.

[2] WAsP, WAsP products, http://www.wasp.dk/Products, 2016.

[3] WindFarmer, http://www.gl-garradhassan.com/ca/software/GHWindFarmer.php, 2016.

[4] WindPRO, http://www.emd.dk/windpro, 2016.

[5] WindFarm, http://www.resoft.co.uk/English/index.htm, 2016.

[6] W.C. Skamarock, J.B. Klemp, J. Dudhia, D.O. Gill, D. Barker, M.G. Duda, X. Huang, W. Wang, A description of the Advanced Research WRF version 3, Technical report NCAR/TN-4751STR, *National Center for Atmospheric Research (NCAR)*, Boulder, CO, 2008.

[7] Lakes Environmental, WRPLOT overview, http://www.weblakes.com/products/wrplot/index.html, 2016.

[8] HOMER Energy, HOMER modules, http://www.homerenergy.com/HOMER_pro_modules.html, 2016.

[9] Natural Resources Analysis, RETScreen overview, http://www.nrcan.gc.ca/energy/software-tools/7465, 2016.

[10] K. Rahmani, A. Kasaeian, M. Fakoor, A. Kosari, S. Alavi, "Wind Power Assessment and Site Matching of Wind Turbines in Lootak of Zabol", *Int. J. Renewable Energy Research*, Vol. 4, No. 4, pp. 965-976, 2014.

[11] S. Goel, S.M. Ali, "Cost analysis of solar/wind/diesel hybrid energy systems for Telecom tower by using HOMER", *Int. J. Renewable Energy Research*, Vol. 4, No. 2, pp. 305-311, 2014.

[12] T.T. Soe, M. Zheng, Z.N. Aung, "Assessment of Economic Feasibility on Promising Wind Energy Sites in Myanmar", *Int. J. Renewable Energy Research*, Vol. 5, No. 2, pp. 548-557, 2015.

[13] A. Acakpovi, "Performance Analysis of Particle Swarm Optimization Approach for Optimizing Electricity Cost from a Hybrid Solar, Wind and Hydropower Plant", *Int. J. Renewable Energy Research*, Vol. 6, No. 1, pp. 323-334, 2016.

[14] Danish Wind Industry Association, http://drømstørre.dk/wp-content/wind/miller/windpower%20web/en/tour/wres/index.htm, 2016.

[15] Suisse Eole, The Swiss wind power data website, Tools overview, http://wind-data.ch/tools, 2016.

[16] L. Lu, H. Yang, J. Burnett, "Investigation on wind power potential on Hong Kong islands—an analysis of wind power and wind turbine characteristics", *Renew Energy*, Vol. 27, No. 1, pp. 1-12, 2002.

[17] A. Al-Mohamad, H. Karmeh, "Wind energy potential in Syria", *Renew Energy*, Vol. 28, pp. 1039-1046, 2003.

[18] A.A. Bhuiyan, A.K.M.S. Islam, A.I. Alam. "Application of Wind Resource Assessment (WEA) Tool: A case study in Kuakata, Bangladesh", *Int. J. Renewable Energy Research*, Vol.1, No.3, pp.192-199, 2011.

[19] G. Gualtieri, "Development and Application of an Integrated Wind Resource Assessment Tool for Wind Farm Planning", *Int. J. Renewable Energy Research*, Vol. 2, No. 4, pp. 674-685, 2012.

[20] J.S. Scire, F.R. Robe, M.E. Fermau, R.J. Yamartino, A User's Guide for the CALMET Meteorological Model (version 5.0), *Earth Tech Inc.*, 1999.

[21] R. Mari, L. Bottai, C. Busillo, F. Calastrini, B. Gozzini, G. Gualtieri, "A GIS-based interactive web decision support system for planning wind farms in Tuscany (Italy)", *Renew Energy*, Vol. 36, pp. 754-763, 2011.

[22] I.M. Essoussi, A. Bouallegue, A. Khedher, "3 kW Wind Turbine Emulator Implementation on FPGA Using Matlab/Simulink", *Int. J. Renewable Energy Research*, Vol. 5, No. 4, pp. 1154-1163, 2015.

[23] J. Manwell, J. McGowan, A. Rogers, *Wind Energy Explained*. Chichester: John Wiley & Sons, UK, 2002.

[24] D.A. Spera, *Wind Turbine Technology: Fundamental Concepts of Wind Turbine Engineering*, 2nd ed. New York: ASME Press, 2009.

[25] J.S. Irwin, "A theoretical variation of the wind profile power law exponent as a function of surface roughness length and stability", *Atmos. Env*., Vol. 13, pp. 191-194, 1979.

[26] S. Rehman, L.M. Al-Hadhrami, M.M. Alam, J.P. Meyer, "Empirical correlation between hub height and local wind shear exponent for different sizes of wind turbines", *Sustainable Energy Technologies and Assessments*, Vol. 4, pp. 45-51, 2013.

[27] N.J. Cook, "The Deaves and Harris ABL model applied to heterogeneous terrain", *J. Wind Eng. Ind. Aerodyn.*, Vol. 66, No. 3, pp. 197-214, 1997.

[28] J. Counihan, "Adiabatic Atmospheric Boundary Layers: A Review and Analysis of Data Collected from the Period 1880-1972", *Atmos. Env*., Vol. 9, pp. 871-905, 1975.

[29] G. Gualtieri, "Atmospheric stability varying wind shear coefficients to improve wind resource extrapolation: A temporal analysis", *Renew Energy*, Vol. 87, pp. 376-390, 2016.

[30] G.A. DeMarrais, "Wind speed profiles at Brookhaven National Laboratory", *J. Meteorol.*, Vol. 16, pp. 181-190, 1959.

[31] M.L. Kubik, P.J. Coker, J.F. Barlow, C. Hunt, "A study into the accuracy of using meteorological wind data to

estimate turbine generation output", *Renew Energy*, Vol. 51, pp. 153-158, 2013.

[32] G.P. Van den Berg, "Wind turbine power and sound in relation to atmospheric stability", *Wind Energy*, Vol. 11, pp. 151-169, 2008.

[33] T. Burton, D. Scarpe, N. Jenkins, E. Bossanyi, *Wind Energy Handbook*, Chichester, UK: John Wiley & Sons, 2001.

[34] R.J. Barthelmie, S.T. Frandsen, M.N. Nielsen, S.C. Pryor, P.-E. Rethore, H.E. Jørgensen, "Modelling and measurements of power losses and turbulence intensity in wind turbine wakes at Middelgrunden offshore wind farm", *Wind Energy*, Vol. 10, pp. 517-528, 2007.

[35] D.L. Elliot, J.B. Cadogan, "Effects of wind shear and turbulence on wind turbine power curves", *European community wind energy conference and exhibition*, Madrid, Spain, 10-14 Sep. 1990.

[36] J. Pramod, *Wind energy engineering*, USA: McGraw Hill, 2011. ISBN: 978-0-07-171478-5.

[37] J. Wieringa, "Gust factors over open water and built-up country", *Boundary-Layer Meteorology*, Vol. 3, pp. 424-41, 1973.

[38] W. Frost, B.H. Long, R.E. Turner, Engineering handbook on the atmospheric environmental guidelines for use in wind turbine generator development, NASA TP-1359, *Lewis Research Center*, Cleveland, OH, 1978.

[39] M. Abbes, J. Belhadj, "Wind resource estimation and wind park design in El-Kef region, Tunisia", *Energy*, Vol. 40, No. 1, pp. 348-357, 2012.

[40] M. Taylor, P. Mackiewicz, M.C. Brower, M. Markus, "An analysis of wind resource uncertainty in energy production estimates", *European wind energy conference (EWEC)*, London, UK, 2004.

[41] S. Siddabathini, T. Sorensen, "Uncertainty of long term correction of wind speed: the importance of consistency of data", *European wind energy conference (EWEC)*, Marseille, France, 2009.

[42] D. VanLuvanee, T. Rogers, G. Randall, A. Williamson, T. Miller, "Comparison of WAsP, MS-Micro/3, CFD, NWP, and analytical methods for estimating sitewide wind speeds", *AWEA wind resource assessment workshop*, Minneapolis, MN, 2009.

[43] P. Spengemann, V. Borget, "Review and analysis of wind farm operational data. Validation of the predicted energy yield of wind farms based on real energy production data", *Proceedings DEWEK*, Vol. 9, 2008.

[44] IEC 61400-1 standards, Wind Turbines–Part 1: Design Requirements. *International Electrotechnical Commission*, 3rd ed. 2005–08. Geneva, Switzerland, 2005.

[45] G. Gualtieri, S. Secci. "Comparing methods to calculate atmospheric stability-dependent wind speed profiles: A case study on coastal location", *Renew Energy*, Vol. 36, pp. 2189-2204, 2011.

[46] G. Gualtieri, G. Zappitelli, "Investigating wind resource, turbulence intensity and gust factor on mountain locations in Southern Italy", *Int. J. of Green Energy*, Vol. 12, No. 4, pp. 309-327, 2014.

[47] G. Gualtieri, "Surface turbulence intensity as a predictor of extrapolated wind resource to the turbine hub height", *Renew Energy*, Vol. 78, pp. 68-81, 2015.